
Contents

1	Introduction	1
1.1	Early Radio Astronomy and Distant Radio Galaxies	1
1.2	High-Redshift Radio Galaxies	2
1.2.1	Characteristics	2
1.2.2	Feedback Processes	5
1.2.3	Open Questions	6
1.3	Active Galactic Nuclei	6
1.4	Low Frequency Carbon Radio Recombination Lines	9
1.4.1	The Cold Neutral Medium	9
1.4.2	Observing Carbon Radio Recombination Lines	10
1.4.3	Theoretical Models	10
1.5	Advances in Low Frequency Radio Astronomy	12
1.6	This Thesis	15
1.7	The Future is Bright at Low Frequencies	18
	Bibliography	25

List of Figures

Chapter 1	1
1.1 Examples of Fanaroff-Riley FRI and FR II sources	3
1.2 The correlation between spectral index and redshift for bright radio galaxies	4
1.3 A diagram of a radio loud high-excitation AGN	8
1.4 LOFAR locations, the Chilbolton station, and LBA dipoles . . .	14

List of Tables

Chapter 1	1
1.1 General properties of different ISM components	11

CHAPTER 1

Introduction

“Space is big. You just won’t believe how vastly, hugely, mind-bogglingly big it is.

*I mean, you may think it’s a long way down the road to the chemist’s,
but that’s just peanuts to space.”*

—Douglas Adams—

1.1 Early Radio Astronomy and Distant Radio Galaxies

Karl G. Jansky was conducting experiments in the early 1930s with telecommunications receivers for the Holmdel Radio Laboratories of Bell Telephone Laboratories, Inc. when he serendipitously detected electromagnetic radiation of an unknown origin. Using the receivers, tuned to frequencies of 20.5 MHz (wavelengths of 14.6m), he tracked the signal for 24 hours approximately once a month during 1932. These observations led Jansky to determine that the origin of the radiation was fixed in space and localized in the direction of the Galactic center. Jansky published his results in 1933. Grote Reber read about Jansky’s discovery and followed it up with observations using a radio telescope of his own design. Reber mapped the Galactic center and a bright source in the direction of the Cygnus constellation at frequencies of 3.3 GHz, 900 MHz, and 160 MHz (Reber, 1949). A census of radio ‘stars’ in the sky began to emerge.

In 1954 Walter Baade and Rudolph Minkowski first associated the radio source in Cygnus with a faint distant galaxy. Based on the distance to the galaxy, Baade and Minkowski came to the conclusion that the total energy of the radio emission was almost 10^{43} ergs s $^{-1}$, larger than the total optical emission. The discovery that galaxies could produce such large amounts of energy revolutionised astronomy, but it would be another 30 years before radio galaxies were placed as important pieces in the overall scheme of galaxy evolution.

Early studies of energetic radio sources and their optical counterparts were enabled by significant advances in radio astronomy over the next few decades.

These advances included the first use of multi-element systems by Ryle and Vonberg in 1946 and the first use of earth rotation synthesis by Ryle in 1962. The work initially focused on cataloguing the brightest sources in the sky at radio frequencies less than 200MHz. Surveys with Cambridge interferometry mainly covered frequencies ranging from 151 to 178MHz (Edge et al., 1959; Bennett, 1962; Pilkington & Scott, 1965). Several surveys were conducted with simple wire or dipole instruments at frequencies less than 100MHz, including surveys from the Cambridge Interferometer at 38MHz (Kellermann et al., 1969); the Clark Lake Radio Observatory at 26.3MHz (Viner & Erickson, 1975); and the Dominion Radio Astrophysical Observatory ‘T-shaped’ radio telescope at 22MHz (Roger et al., 1986).

The surveys revealed different types of radio sources. Many bright, powerful radio sources consisted of radio jets up to hundreds of times larger than their optical host galaxies. Fanaroff & Riley (1974) sorted these extended radio sources into two classes based on their morphological features. Fanaroff-Riley I (FRI) sources consist of radio jets that are more like fountains, with wider opening angles and dimmer radio luminosities towards their extremities. Fanaroff-Riley II (FRII) sources have highly collimated radio jets that are edge brightened where the jets terminate. An example of each class is shown in Figure 1.1. Generally FRI sources have lower radio powers ($\lesssim 10^{25} \text{ W Hz}^{-1}$ at 1.4GHz) and it is thought that the jet power as well as the ambient density play a role in whether a highly collimated jet will remain collimated and turn into an FRII source or be disrupted and change into an FRI source (e.g., Kaiser & Best, 2007). In cases where the ambient density is asymmetric, hybrid sources with characteristics of both FR classes can be observed.

Until the mid-1980’s radio galaxies were seen merely as exotic high-energy phenomena that were useful as a way to refine searches for distant optical host galaxies (e.g., Smith & Spinrad, 1980). In particular, a correlation emerged where radio sources with ultra-steep spectral indices ($\alpha > 1$, where flux density $S \propto \nu^{-\alpha}$) were more likely to be found at higher redshifts, see Figure 1.2 (Tielens et al., 1979; Blumenthal & Miley, 1979). This correlation has been successfully exploited to push the limit for finding massive galaxies at high redshift (e.g. Röttgering et al., 1994).

1.2 High-Redshift Radio Galaxies

1.2.1 Characteristics

The unexpected discovery in 1987 of an alignment between the radio jets and optical continuum emission for radio galaxies at $z \geq 0.7$ changed the entire way

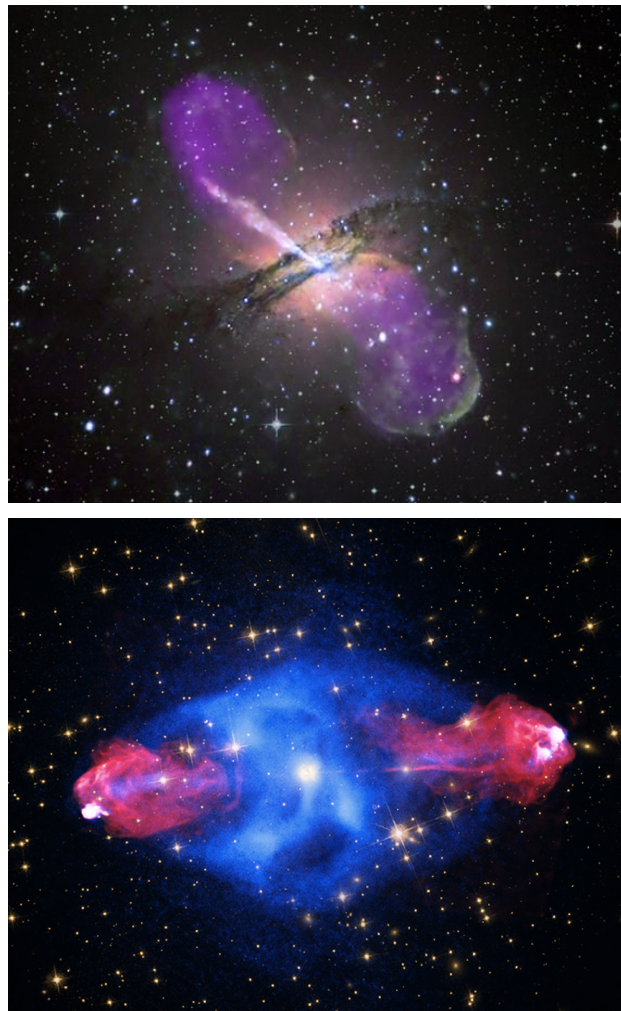


Figure 1.1: Composite images showing examples of typical Fanaroff-Riley FRI and FRII sources. *Top:* A composite image of FRI radio galaxy Centaurus A. The color purple shows the radio emission which is brighter along the jets towards the host radio galaxy, with fainter emission at the ends of the jets (Credit: X-ray: NASA/CXC/CfA/R.Kraft et al; Radio: NSF/VLA/Univ.Hertfordshire/M.Hardcastle; Optical: ESO/WFI/M.Rejkuba et al.). *Bottom:* Radio galaxy Cygnus A, the archetypal FR II radio galaxy. The color red shows the edge-brightened radio emission. The X-ray emission shown in blue traces the cocoon of shocked jet material and intergalactic medium (X-ray: NASA/CXC/SAO; Optical: NASA/STScI; Radio: NSF/NRAO/AUI/VLA).

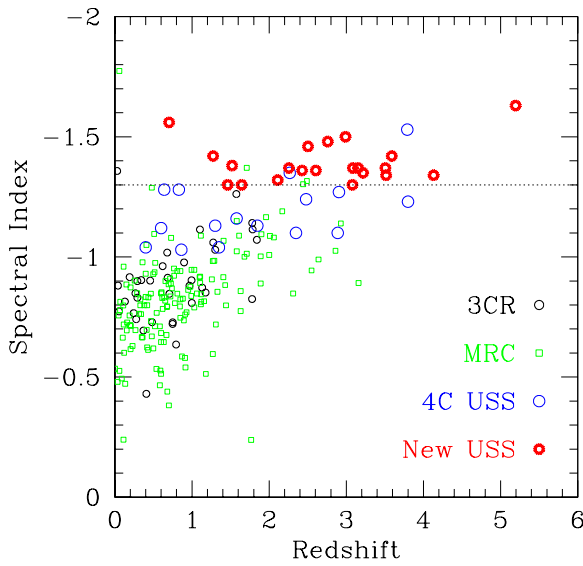


Figure 1.2: The correlation between spectral index and redshift seen for bright radio galaxies. Plot from De Breuck et al. (2000).

radio galaxies were seen (Chambers et al., 1987; McCarthy et al., 1987). Two things became clear: first, that the radio jets interact with their host galaxy and could possibly impact its evolution; and second, that high redshift radio galaxies might be fundamentally different sources than local radio galaxies, where the alignment effect is not observed. High-redshift radio galaxies (HzRGs, defined here as having $z \geq 2$) became the subject of intense multi-wavelength studies during the 1990s and 2000s. Often found surrounded by over-densities of galaxies indicating the presence of a proto-cluster, HzRGs are now thought to evolve into the most massive galaxies in the present-day Universe (e.g., Pentericci et al., 2000; Hatch et al., 2011). They are therefore important beacons for studying the evolution of galaxies as they traverse into clusters of galaxies, which are the largest gravitationally bound objects in the Universe.

HzRGs exhibit characteristics that indicate an interaction with their host galaxies, providing a feedback mechanism by which the radio jets can influence galaxy evolution. The optical morphologies of HzRGs are clumpy and extended along the radio jet axis (e.g., Pentericci et al., 1998, 1999). Many HzRGs are embedded in huge Lyman- α haloes, indicating the presence of ionised gas (e.g., Humphrey et al., 2007). Emission lines other than Lyman- α are present and also extended along the jet axis (Motohara et al., 2000; Humphrey et al.,

2007). The kinematics indicated by these emission lines provide evidence for both an infalling quiescent halo (e.g., Villar-Martín et al., 2003; Humphrey et al., 2007) and turbulent outflows (Villar-Martín et al., 1999; Humphrey et al., 2006). Asymmetries in the radio lobes have been linked to properties of the emission lines. Humphrey et al. (2007) found that Lyman- α was always brighter in relation to other emission lines on the side of the brighter radio lobe. The spatial correlation of the emission line properties with the radio jets is strong evidence for feedback between radio jets and the host galaxy.

1.2.2 Feedback Processes

The alignment of optical continuum and the radio jets in HzRGs is not the only indication that radio jets can interact with their host galaxies. Radio jets are powered by super-massive black holes at the centre of their host galaxies. There are observed correlations between the mass of the super-massive black hole and properties of the host galaxy such as velocity dispersion (e.g., Ferrarese & Merritt, 2000; Gebhardt et al., 2000), bulge mass (e.g., Kormendy & Richstone, 1995; Magorrian et al., 1998), and galaxy luminosity (e.g., Marconi & Hunt, 2003; Gürtekin et al., 2009). These correlations indicate that the super-massive black hole and its host galaxy co-evolve. Radio jets can play a part in this co-evolution, either by jet-induced star formation or by regulation of star formation via heating of cold gas that would otherwise condense into stars.

Radio jets can drive shocks into the interstellar medium, enhancing star formation by increasing turbulent pressure and compressing clouds that then form stars (e.g., Silk & Nusser, 2010). Observational evidence for this ‘positive’ feedback can be found in both nearby sources (e.g., Blanco et al., 1975; Donahue et al., 2002; Inskip et al., 2008) as well as HzRGs (Chambers et al., 1987; Inskip et al., 2005).

There can also be ‘negative’ feedback from radio jets heating up cold gas and suppressing star formation (e.g., Best et al., 2005a; Hardcastle et al., 2013). The jets can also be responsible for expelling molecular gas from the host galaxy, depleting the necessary fuel to form stars (e.g., Feruglio et al., 2010; Dasyra & Combes, 2012; Tadhunter et al., 2014). Cosmological simulations often invoke negative feedback to quench star formation in massive galaxies, bringing the simulations in line with observations of ‘red and dead’ massive galaxies (e.g., Bower et al., 2006; Werner et al., 2014).

1.2.3 Open Questions

Although HzRGs have been the topic of intense multi-wavelength study, many questions still remain open (for a complete list see Miley & De Breuck, 2008). One of the biggest mysteries is why HzRGs have much steeper radio spectra than their low-redshift counterparts. Although this has been a topic of intense study (e.g., Athreya & Kapahi, 1998; Blundell et al., 1999; Klamer et al., 2006) it is still unclear if the dominant cause of the relation between spectral index and redshift is observational or due to different particle acceleration mechanisms in the relativistic plasma of the radio jets. Could steeper spectra be caused by interaction with a denser ambient environment? If so, what are the detailed processes by which the jets interact with their environments? How exactly does feedback between the host galaxy and the energetic processes associated with the radio jets impact the galaxy's evolution? The vigorous star formation and the jets themselves have to be fuelled, but not all gas phases present in HzRGs are well constrained. In particular, it is important to characterise the molecular and cold gas content of HzRGs.

This thesis aims to provide new low radio frequency information on the particle acceleration mechanisms present in HzRGs and lay the foundation for studying the cold gas content of HzRGs via observations of low frequency carbon radio recombination lines. The rest of this chapter will outline for the reader the relevant topics of active galactic nuclei and low frequency carbon radio recombination lines.

1.3 Active Galactic Nuclei

In 1963 the Dutch astronomer Maarten Schmidt observed the spectrum of the unresolved optical counterpart of the bright radio source 3C 273. The measured cosmological redshift $z = 0.158$ revealed that the compact optical source, identified as the nuclear region of a galaxy, was 100 times brighter than other luminous galaxies associated with radio galaxies that were known at the time. While searching for the optical counterparts to other radio sources in the Third Cambridge catalogue, many optical plates also showed objects with a similar optical properties but no radio counterpart. This led to the first identification of a class of quasi-stellar galaxies (now called quasars) by Sandage in 1965.

Today we understand that quasars are a subset of a larger class of galaxies which have an Active Galactic Nucleus (AGN). The excess energy in AGN is powered by gas drawn into the deep potential well created by a central super-massive black hole of masses millions to tens of billions times that of the Sun. Almost every massive galaxy has a super-massive black hole at its centre. The

observational characteristics that distinguish AGN from normal galaxies are varied, and can include radio emission, superlatively high luminosities, strong emission lines from ionised gas, detections from compact X-ray sources, and the presence of polarised light. Not every AGN exhibits the same characteristics, and even individual objects may show variability on observable time scales.

AGN can be broadly classed into two categories. The first category is typically referred to as ‘high-excitation’, ‘quasar-mode’, ‘radiative-mode’, or ‘strong-lined’ and these objects are governed by what is called cold-mode accretion. In this accretion mode the AGN activity is fuelled by a large central repository of cold gas (e.g, Larson, 2010). A depiction of this type of AGN is shown in Figure 1.3. The super-massive black hole is thought to be surrounded by an accretion disk which produces optical through ultraviolet thermal emission in a region only a few parsecs across, giving rise to the compact ‘quasi-stellar’ appearance first noted by Schmidt. A hot corona above the accretion disk produces X-ray radiation via inverse Compton scattering. The strong radiation produced by the optical through X-ray light photoionizes the area directly surrounding the accretion disk. Outside this area is a dusty molecular torus that obscures the radiation from the accretion disk when viewed edge-on, but will re-radiate the absorbed emission in the mid-infrared. Near the accretion disk is gas with velocity dispersions of a few thousand kilometers per second, which produces broad emission lines (the broad line region). Slower, cooler gas that extends well beyond the torus produces narrow emission lines (the narrow line region). Radio jets are only present in a fraction of the sources.

In unification models, the viewing angle towards the AGN results in different observed features (e.g., Barthel, 1989; Antonucci, 1993; Urry & Padovani, 1995). When viewed edge-on the torus will obscure the emission from the accretion disk, causing the optical quasar to be hidden. The broad line region will also be hidden, and only narrow emission lines will be seen. AGN that are tilted so the observer sees inside the torus will be seen as classical optical quasars, and both broad and narrow lines will be present. If a radio jet is present the radio emission may be beamed towards the observer, causing apparent super-luminal motion (Barthel et al., 1989). The high occurrence of beamed radio emission in quasars has led to the wide acceptance of unified models of radio galaxies and quasars (Barthel, 1989).

The second category of AGN are termed ‘low-excitation’, ‘radio-mode’, ‘radiatively inefficient’, or ‘weak-lined’ AGN. In these objects the fuel source has been argued to be hot gas (e.g., Hardcastle et al., 2007), which is accreted via advection dominated accretion or radiatively inefficient accretion flows (e.g.,

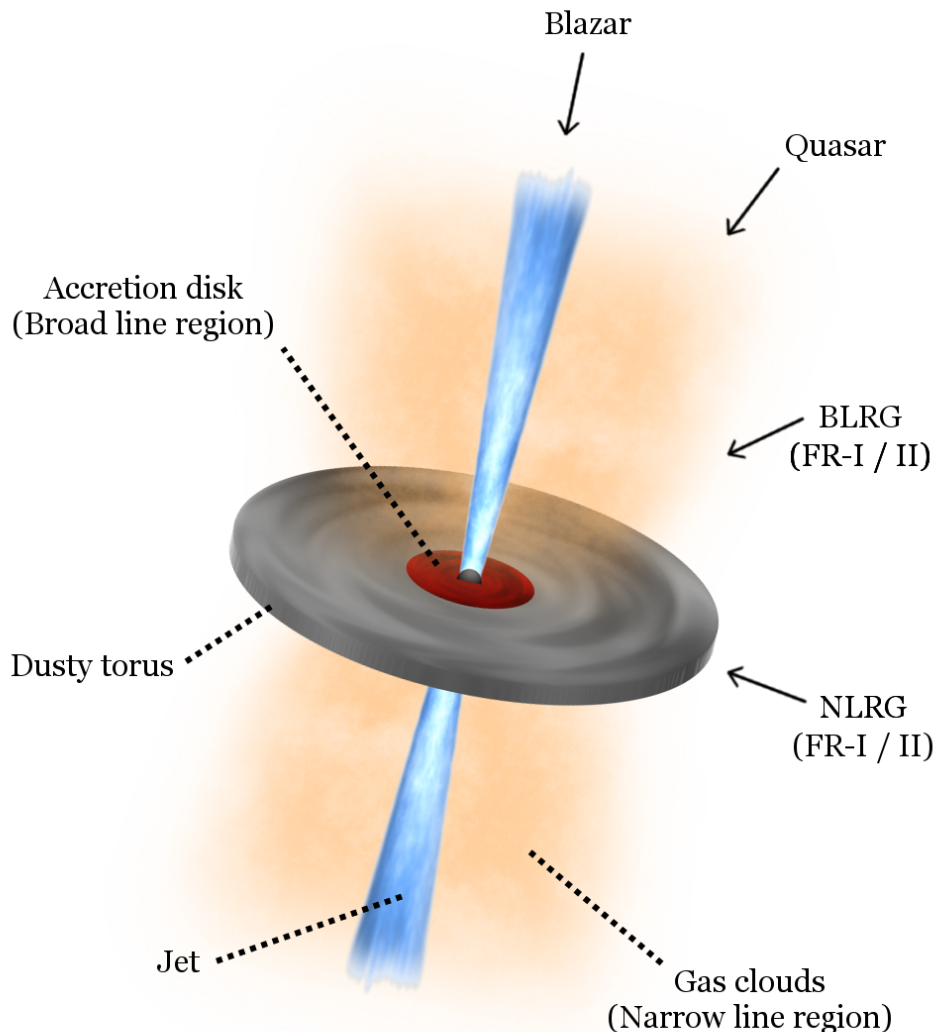


Figure 1.3: A diagram of a radio loud high-excitation AGN. The jet is not present in radio quiet AGN. The arrows indicate the type of object that is seen based on viewing angle. Image credit J. Harwood.

Narayan & Yi, 1994; Quataert, 2001; Ho, 2008). Almost all available energy from accretion is channelled into jets. Low excitation AGN lack the strong emission lines associated with the high-excitation AGN (e.g. Hine & Longair, 1979; Jackson & Rawlings, 1997), and evidence for an obscuring torus is not present (e.g., Whysong & Antonucci, 2004; Ogle et al., 2006). Observed X-ray emission is consistent with jets rather than accretion (Hardcastle et al., 2006; Evans et al., 2006), and the accretion disk is either missing or truncated. The types of galaxies that host low-excitation AGN are typically massive, red galaxies in dense environments (Best et al., 2005b).

Both high-excitation radio galaxies (HERGs) and low-excitation radio galaxies (LERGs) are found in radio surveys. LERGs comprise almost the entire population of low-luminosity radio AGN with powers $\lesssim 10^{25} \text{ W Hz}^{-1}$ at 1.4GHz in the local Universe, while HERGs begin to dominate the population of radio AGN with powers $> 10^{26} \text{ W Hz}^{-1}$ (Best & Heckman, 2012). This is suggestive of the same type of power division between FRI and FRII sources, but not all HERGs have FRII morphology, and not all LERGs have FRI morphology. Best & Heckman (2012) found that HERGs and LERGs are better separated by their accretion rates, with Eddington accretion rates of 1-10 per cent for HERGs and less than 1 per cent for LERGs.

1.4 Low Frequency Carbon Radio Recombination Lines

1.4.1 The Cold Neutral Medium

The cycle of star formation plays a key part in shaping a galaxy's evolution. The interstellar medium (ISM) provides the fuel to make new stars and is the repository for the ejecta of old stars. The ISM is recycled through many different components, and the main components are summarised in Table 1.1. While many of these components have been well characterised, constraining the physical properties (n_e, T_e) of the cold neutral medium (CNM) has remained challenging. This cold, diffuse phase of the ISM has historically been studied via the spin-flip transition of neutral hydrogen that manifests as emission or absorption at 21 cm (1.4GHz). Constraining the physical parameters of the CNM via H I observations is difficult, and limited to only certain conditions where additional information to separate the CNM from the warm neutral medium is available (e.g., Heiles & Troland, 2003).

Carbon radio recombination lines (CRRLs) offer another means to observe the CNM. The ionisation potential of carbon is less than that of hydrogen and thus singly-ionised carbon can co-exist with neutral hydrogen. In low temperature and density conditions, electrons can recombine with C⁺ to very high quan-

tum levels ($n \gtrsim 300$), producing recombination lines at low radio frequencies ($\nu \lesssim 240\text{MHz}$).

1.4.2 Observing Carbon Radio Recombination Lines

CRRLs have been observed in our own Galaxy on scales of degrees along the Galactic plane (e.g., Erickson et al., 1995; Kantharia & Anantharamaiah, 2001), and on smaller scales in the direction of bright background sources such as H II regions (e.g., Golykin & Konovalenko, 1991), Cassopeia A (e.g., Asgekar et al., 2013; Payne et al., 1989; Konovalenko & Sodin, 1981), and extragalactic sources (Oonk et al., 2014). Only hydrogen recombination lines have been detected at frequencies $> 1\text{GHz}$ in extragalactic sources, all of which are bright, nearby starburst galaxies (e.g., Shaver et al., 1977; Anantharamaiah et al., 1993; Rodriguez-Rico et al., 2004; Roy et al., 2008). These high-frequency extragalactic detections are all most likely associated with H II regions rather than the CNM.

Observing CRRLs at low frequencies has three main advantages. First, their optical depth will be higher which makes detection easier. In particular, the stimulation of the ground state of carbon (${}^2\text{P}_{1/2} \rightarrow {}^2\text{P}_{3/2}$) can be coupled with the recombination of an electron to an extremely high quantum level. Second, the number of lines per unit frequency increases with decreasing frequency and wide bandwidth instruments can observe multiple CRRLs simultaneously. Over small enough ranges in frequency, the line profiles will be correlated, and stacking procedures can be used to procure a CRRL detection even when the lines are not detected individually. Even though CRRLs are more closely spaced at lower frequencies, they are intrinsically narrow lines and are unlikely to be blended even at the lowest observable frequencies. Third, low-frequency CRRLs are seen in absorption, opening the possibility of observing the CNM even in bright objects at high redshift (Shaver, 1978).

1.4.3 Theoretical Models

Once detected, comparison of the measured line profiles with detailed theoretical models can constrain the physical properties of the CNM (e.g., Shaver, 1975b; Payne et al., 1989, 1994). CRRLs come from singly ionised carbon with an electron recombining at a very high quantum level. Such a system can be approximated as a Rydberg atom. The optical depth of the CRRLs can be related to the ‘departure coefficient’ which describes the deviation of the level population from local thermodynamic equilibrium (LTE). Early models were developed for Rydberg atoms which were limited at the time to quantum levels

Table 1.1: General properties of different interstellar medium components (adapted from Cox, 2000).

Phase	State of H	Density [cm ⁻³]	Temperature [K]	Heating	Cooling
Molecular Clouds	H ₂	>100	10–20	Cosmic Rays	CO, FIR
H II Regions	H II	>100	10 ⁴	Photoionization	[O III], [O II], H recombination
Cold Neutral Medium	H	0.01–1.0	10–300	Photoelectrons from dust	[C II]
Warm Neutral Medium	H	0.1–10	≈8000	Photoelectrons from dust	[C II]
Warm Ionised Medium	H II	0.3–10	≈8000	Photoionization	Hα, [N II], [S II]
Hot Ionised Medium	H II	0.01	>10 ^{5.5}	Shocks	X-rays

$n \lesssim 500$ (e.g., Seaton, 1964; Dupree, 1969; Shaver, 1975a; Salem & Brocklehurst, 1979; Storey & Hummer, 1991).

A major advancement in the last thirty years was the inclusion of the dielectronic recombination, a process by which the stimulation of the ground state of carbon is coupled with the recombination of an electron to very high quantum levels (e.g., Walmsley & Watson, 1982; Ponomarev & Sorochenko, 1992). Most recently, these models have been updated making use of advances in computing. Salgado et al. (2016a) improved the theoretical models in several ways, including: updated values for the necessary rates used to calculate the level populations; proper treatment of dielectronic recombination by explicitly computing level populations for l quantum levels; and calculations of level populations up to quantum levels up to $n = 10000$. These updated models are necessary to provide sound theoretical predictions for CRRL intensities, which originate in low temperature and low density gas (Salgado et al., 2016b). The theoretical models provide an excellent foundation for future studies of low-frequency CRRLs, and will be used in the coming years to characterise the CNM in the Galaxy as well as extragalactic sources.

1.5 Advances in Low Frequency Radio Astronomy

During the last fifty years, astronomers have pushed to higher frequencies (above 1 GHz) where better resolution and sensitivity were easier to achieve. Recently there has been a resurgence of interest in low-frequency radio astronomy. The upcoming Square Kilometre Array (SKA; Schilizzi, 2005) will mark a new era for radio astronomy with unprecedented sensitivity at metre to centimetre wavelengths. Its development has led to a rapid growth in antenna design and improvements in interferometer back-ends. Several pathfinder arrays have been constructed, including the Australian SKA Pathfinder (ASKAP; Johnston et al., 2007), the South African SKA precursor MeerKAT (Gibbon et al., 2015). A system of low-frequency dipoles were installed at the primary foci of the Very Large Array (VLA) antennas and used to survey the sky north of -30 degrees declination at 74 MHz (Cohen et al., 2007).

Advances in computing have also allowed for significant improvements without replacing front end hardware. Updated backend instrumentation has transformed the VLA into the Karl G. Jansky VLA (VLA; Perley et al., 2004) with improvements in both its frequency coverage and sensitivity. Computing advances have also allowed for the correlation of signals from hundreds to thousands of individual elements. This has revolutionized low-frequency radio astronomy, and several dipole-array interferometers have been constructed, in-

cluding the Murchison Widefield Array (MWA; Tingay et al., 2013), the Long Wavelength Array (LWA; Taylor, 2007), and the Low Frequency Array (LOFAR; van Haarlem et al., 2013).

LOFAR is a new radio telescope with a revolutionary phased-array design that makes use of electronically pointed dipoles rather than traditional dish telescopes. The simple dipole antennas are grouped into stations. There are 37 stations concentrated in the Netherlands, and 12 stations spread across five other European countries. There are two different types of dipoles in each station. The High Band Array (HBA) operates at 110 – 240 MHz and consists of thin metal dipoles supported by Styrofoam and protected from the weather. The Low Band Array (LBA) which is the focus of this thesis operates at 10 – 90 MHz with a sharply peaked response making the array most sensitive around 60 MHz. Each LBA antenna consists of two simple wire dipoles (one for each linear polarisation) attached to the ground and supported at their apex in the center by a plastic pipe. The station locations are shown in Figure 1.4, along with a bird’s eye view of a station, and a close up of the LBA dipoles.

The signals from each antenna are converted to digital and then the station is pointed electronically by introducing phase delays in the signal path before station summation. The digital nature of the signals allows multiple beams to be formed simultaneously, limited only by the total bandwidth of the instrument. When combined with its large instantaneous field of view, this makes LOFAR an extremely efficient survey instrument. Up to 96 MHz of bandwidth is available to be divided amongst different beams or concentrated in one beam for increased sensitivity. This bandwidth is divided into subbands, which can be sub-divided into channels of specified widths as small as 767.9 Hz in routine observations (making LOFAR an ideal instrument for observing CRRLs).

Most LOFAR observations use only the stations in the Netherlands, which provide fields of view of tens of square degrees and resolutions of a few arcseconds (HBA) to tens of arcseconds (LBA). The wide geographic distribution of international stations provides LOFAR with an effective collecting area more than a thousand kilometres across, allowing sub-arcsecond resolution to be achieved. This capability sets LOFAR uniquely apart from other low-frequency arrays, and enables exploration of entirely different science topics.

With new technological advances come new challenges. Low frequency radio telescopes operate in a regime where the ionosphere can have a large impact on observations, causing stationary radio sources to appear to move and/or scintillate in an image, directly comparable to the same problems due to seeing in the optical regime. With the wide fields of view afforded by low-frequency tele-



Figure 1.4: *Top:* The locations of LOFAR stations. The data in this thesis were taken before the stations in Poland were constructed, when the longest baseline was between Onsala and Nançay (1292km). *Middle:* The LOFAR-UK station at Chilbolton. The LBA antennas are in the foreground with the HBA antennas clustered together under a weather-protective covering behind the LBA. *Bottom:* Dipoles from an LBA station within the central core of LOFAR, with the author in the picture for scale.

scopes, the assumption that a single correction is valid for the entire field of view breaks down, and new calibration techniques are necessary.

A substantial amount of progress has been made in calibration techniques since the early days of radio astronomy. From self-calibration on individual sources in small fields of view (e.g., Pearson & Readhead, 1984) to the development of field-based calibration (Cotton et al., 2004) using multiple sources in large fields of view, the scope of calibration techniques has expanded. This is particularly relevant for LOFAR, where the ionosphere, and to a lesser extent imperfect beam models, can cause direction-dependent distortions. Intema (2009,2014) developed the Source Peeling and Atmospheric Modelling (SPAM) technique to deal with ionospheric issues for the Giant Metrewave Radio Telescope, which operates at frequencies from 150 to 610MHz. The most recent advancements for calibrating LOFAR data to make wide-field images have been SAGECal (Yatawatta et al., 2013; Kazemi et al., 2011) and facet calibration (van Weeren et al., 2016; Williams et al., 2016).

Using the full International LOFAR requires different calibration schemes, as it is challenging to combine signals from geographically isolated stations. Errors in station positions, different station clocks, and errors from propagation through different atmospheric conditions must all be accounted for. The ionosphere dominates the delay (how phase changes with frequency) errors in the low-frequency regime. The delay errors have ν^{-2} dependence on ionospheric conditions, making it even more challenging to calibrate data for the LBA than the HBA. With some modifications the global fringe-fitting algorithm described by Cotton (1995) has been successfully used for LOFAR HBA (Varenius et al., 2015; Moldón et al., 2015; Varenius et al., 2016).

Finally, LOFAR is pushing forward the development of fast algorithms to deal with large volumes of data, in preparation for the Tier 1 survey of the entire Northern sky (north of 0 degrees declination). One major improvement was the implementation of the Statistically Efficient and Fast Calibration (StEfCal; Salvini & Wijnholds, 2014) in the native LOFAR software. The use of Kalman filters is a promising step forward into the next generation of efficient calibration for the unique problems of low-frequency radio astronomy (Smirnov & Tasse, 2015).

1.6 This Thesis

HzRGs are spectacular objects with clear interaction between the radio jets and their host galaxies and environments. The goal of this thesis is to use low frequency radio astronomy tools to help answer the following questions:

- Are HzRGs fundamentally different objects than their low redshift counterparts?
- What are the mechanisms that cause the correlation between radio galaxy spectral index and redshift?
- What is the cold gas content in extragalactic radio sources, and how does it play a part in the cycle of star formation?

In particular, the tools used are catalogues from deep, wide-field LOFAR imaging; the highest resolution images at frequencies less than 100MHz using the international LOFAR LBA stations; and finally, spectroscopic observations with both LOFAR and the Karl G. Jansky VLA (VLA).

Chapter 2 begins with a catalogue of LOFAR-detected radio sources from Williams et al. (2016). Cross-matching with the AGN and Galaxy Evolution Survey (AGES; Kochanek et al., 2012) multi-wavelength data provides spectroscopic redshifts for 60 radio sources above a power of $10^{25.5} \text{ W Hz}^{-1}$. Optical and near-infrared quasar identifications are used to separate the sample into radio galaxies and quasars. In orientation-only unification schemes, this is the difference between a viewing angle seeing the obscuring torus edge on (radio galaxy) or being able to see the accretion disk inside the torus (quasar). The sizes of the radio jets will be foreshortened in the latter case, and two samples are compared to test whether or not the difference in sizes is due to orientation effects. The quasar sizes are on average smaller than the radio galaxy sizes by a factor of 3.1 ± 1.0 for the LOFAR-detected radio sources, which is evidence for orientation-based unification.

Chapter 3 is a detailed study at 55MHz of 4C 43.15, one of a sample of 10 high redshift radio galaxies that will be used to examine the spectral index–redshift correlation. This chapter makes use of traditional very long baseline interferometry (VLBI) techniques to make the highest resolution images below 100MHz, achieving sub-arcsecond resolution with the International LOFAR. When coupled with archival VLA observations, the images of this $z = 2.4$ radio galaxy reveal a bridge of emission between the two FRII radio lobes. The morphology and spectral index properties of 4C 43.15 are similar to those seen in local radio galaxies. The integrated spectra of the radio lobes show a break at frequencies between 55MHz and 1.4GHz, with steepening at higher frequencies. This indicates that the original classification as an ultra steep spectrum radio galaxy was dependent on the fixed observing frequencies, which straddled the break in the spectrum.

The observed correlation between radio spectral index and redshift has been successfully used to find high redshift radio galaxies like the one studied in Chapter 3. However the cause of the relation is still unclear. **Chapter 4** investigates whether the relation between spectral index and redshift ($\alpha - z$) can arise simply due to the increased photon energy density of the cosmic microwave background (CMB), which increases as $(1 + z)^4$. This causes increased synchrotron losses. This chapter uses a new approach of selecting archival data for ~ 50 radio galaxies at $z \leq 1$ with enough data for spectral modelling, and simulating radio spectra of radio galaxies at higher redshifts. This allows for the introduction of only the inverse Compton losses to see if this effect alone can reproduce the $\alpha - z$ relation. Observational selection effects are used so the simulated sample can be compared to an observed sample. We find that the observed relation can be entirely reproduced with only the increased synchrotron losses due to inverse Compton scattering of photons from the CMB at high redshift, without having to invoke any intrinsic α -power relationship or environmental effects.

Chapter 5 presents the first detection of extragalactic CRRLs, in nearby starburst galaxy M82. Starburst galaxies are undergoing intense, short-lived periods of star formation with star formation rates up to tens to hundreds of solar masses per year. Normal galaxies maintain star formation rates of 1 – 5 solar masses per year. Starburst events are often found in disturbed galaxies where there is evidence of a merger. The M82 starburst was likely triggered by an interaction with M81 (Yun et al., 1993). The 8.5σ detection is achieved by stacking 22 α transitions ($\Delta n = 1$) in the range of 50–64 MHz using LOFAR LBA observations. The CRRLs are detected in absorption, and should be detectable if present in high redshift radio galaxies with similar flux densities. The line profile has a peak optical depth of 3×10^{-3} and a full width half maximum of 31 km s^{-1} . The narrow line width suggests that the line is localized to a small region of M82, as other gas tracers like CO show widths of $\sim 200 \text{ km s}^{-1}$. The centroid velocity suggests that the line is associated with the nuclear region. The line profile suggests that the CRRL originating gas is associated with the cold atomic gas in the direction of the nuclear region.

The CRRL detection described in Chapter 5 is not enough to constrain the models of gas temperature and density, and in **Chapter 6** spectroscopic observations with the VLA P-band are used to rectify this. The CRRLs in this frequency range (250–480 MHz) are expected to be in emission. We find a meaningful upper limit to the optical depth, and constrain the gas temperature and density using the previous detection and this new upper limit. We find that the gas tem-

perature and density are $T_e = 95^{+105}_{-85}$ K and $n_e = 0.030 \pm 0.005 \text{ cm}^{-3}$. These gas temperatures are consistent with Galactic values for the cold neutral medium. We estimate an upper limit on the C II/H I ratio of 1.05×10^{-3} .

Chapter 7 describes the calculation of bound-bound Gaunt factors for quantum levels up to $n = 2000$. These factors are used to calculate oscillator strengths, one of the necessary quantities in the updated theoretical models of CRRLs Salgado et al. (2016a,b). A review is presented of various calculation methods, with particular attention given to the computational problems that led previous authors to use approximations with errors up to ~ 8 per cent. These new calculations have a relative error of 3×10^{-3} when compared with more detailed calculations for low quantum numbers using relativistic corrections. The values are useful for a wide range of physical applications, and are tabulated and published online.

The **Appendices** describe LOFAR commissioning work in support of this thesis, in particular Chapter 3. Appendix A covers simulations showing that bright, off-axis sources can have a large impact on baselines to International LOFAR stations. This is due to a lack of high-resolution models of these bright sources, which are necessary to remove their effects from the data. Appendix B describes challenges faced and their resolution when using the ‘Station Adder’ algorithm used to combine visibilities on particular baselines in Chapter 4. An additional improvement of ~ 1 per cent in the image noise was found to be achieved when using the weighted geometric average of data coordinates, and this improvement was added to the LOFAR *new default pre-processing pipeline* (NDPPP) software.

1.7 The Future is Bright at Low Frequencies

Low-frequency radio astronomy is a rapidly growing field. Even when new instruments like the SKA are fully operational, LOFAR will remain a unique and powerful instrument. In particular, there is no planned instrument that will match the frequency coverage of the LBA (10–90MHz) and the exquisite sub-arcsecond resolution achievable by using International LOFAR.

Chapter 4 laid out the method for using VLBI techniques at frequencies ~ 60 MHz. This provides one data point for one source; the next step is to apply this method to observations of other HzRGs. VLBI observations with the HBA will provide another measurement at frequencies around 150MHz, which is critical to anchor spectral fitting to determine properties of HzRGs. It will be particularly interesting to determine the spectral ages and how they evolve along the jet axes, and to determine the particle acceleration mechanisms present

where the jets terminate. A sample of 10 sources is enough to identify trends for the larger population of HzRGs, which will guide future studies.

The potential to probe the CNM in HzRGs is also thrilling. The detection of CRRLs in Chapter 5 shows that this can be done. HzRGs are known to contain extended gas in several phases (Miley & De Breuck, 2008), and are ideal candidates for CRRL searches. Detections would provide a unique tracer for the cold gas in HzRGs.

There are many other science cases that become possible with the high resolution capabilities of LOFAR. The physics of hot-spots in FRII radio galaxies can be studied in exquisite detail. High resolution images of radio sources will allow star-forming galaxies and AGN to be distinguished on the basis of morphology. Populations of radio-loud AGN with resolved jets can be studied out to redshifts of ~ 2 with the LOFAR Tier 1 survey depths, to see if their evolution evolves with time and/or environment.

One of the most compelling advantages of LOFAR is its survey efficiency. The LOFAR Tier 1 Survey will nicely fill in the $P - z$ diagram for radio galaxies and quasars, providing robust statistics to disentangle orientation effects from physical properties of radio-loud AGN and quasars. This requires supporting spectroscopic redshifts and host galaxy classification, which will be accomplished over the next few years for hundreds of thousands of LOFAR-detected sources using the William Herschel Telescope Enhanced Area Velocity Explorer (WEAVE). The combination of LOFAR data with optical information will provide a powerful tool that will have a lasting impact on the field of galaxy evolution.

Bibliography

- Anantharamaiah K. R., Zhao J.-H., Goss W. M., Viallefond F., 1993, ApJ, 419, 585
- Antonucci R., 1993, ARA&A, 31, 473
- Asgekar A., et al., 2013, A&A, 551, L11
- Athreya R. M., Kapahi V. K., 1998, Journal of Astrophysics and Astronomy, 19, 63
- Baade W., Minkowski R., 1954, ApJ, 119, 206
- Barthel P. D., 1989, ApJ, 336, 606
- Barthel P. D., Hooimeyer J. R., Schilizzi R. T., Miley G. K., Preuss E., 1989, ApJ, 336, 601
- Bennett A. S., 1962, MNRAS, 125, 75
- Best P. N., Heckman T. M., 2012, MNRAS, 421, 1569
- Best P. N., Kauffmann G., Heckman T. M., Ivezić Ž., 2005a, MNRAS, 362, 9
- Best P. N., Kauffmann G., Heckman T. M., Brinchmann J., Charlot S., Ivezić Ž., White S. D. M., 2005b, MNRAS, 362, 25
- Blanco V. M., Graham J. A., Lasker B. M., Osmer P. S., 1975, ApJL, 198, L63
- Blumenthal G., Miley G., 1979, A&A, 80, 13
- Blundell K. M., Rawlings S., Willott C. J., 1999, AJ, 117, 677
- Bower R. G., Benson A. J., Malbon R., Helly J. C., Frenk C. S., Baugh C. M., Cole S., Lacey C. G., 2006, MNRAS, 370, 645
- Chambers K. C., Miley G. K., van Breugel W., 1987, Nature, 329, 604
- Cohen A. S., Lane W. M., Cotton W. D., Kassim N. E., Lazio T. J. W., Perley R. A., Condon J. J., Erickson W. C., 2007, AJ, 134, 1245
- Cotton W. D., 1995, in Zensus J. A., Diamond P. J., Napier P. J., eds, Astronomical Society of the Pacific Conference Series Vol. 82, Very Long Baseline Interferometry and the VLBA. p. 189

- Cotton W. D., Condon J. J., Perley R. A., Kassim N., Lazio J., Cohen A., Lane W., Erickson W. C., 2004, in Oschmann Jr. J. M., ed., SPIE Vol. 5489, Ground-based Telescopes. pp 180–189, doi:10.1117/12.551298
- Cox A. N., 2000, Allen's astrophysical quantities
- Dasyra K. M., Combes F., 2012, A&A, 541, L7
- De Breuck C., van Breugel W., Röttgering H. J. A., Miley G., 2000, AAPS, 143, 303
- Donahue M., Smith B. J., Stocke J. T., 2002, AJ, 123, 1922
- Dupree A. K., 1969, ApJ, 158, 491
- Edge D. O., Shakeshaft J. R., McAdam W. B., Baldwin J. E., Archer S., 1959, Memoirs of the RAS, 68, 37
- Erickson W. C., McConnell D., Anantharamaiah K. R., 1995, ApJ, 454, 125
- Evans D. A., Worrall D. M., Hardcastle M. J., Kraft R. P., Birkinshaw M., 2006, ApJ, 642, 96
- Fanaroff B. L., Riley J. M., 1974, MNRAS, 167, 31P
- Ferrarese L., Merritt D., 2000, ApJL, 539, L9
- Feruglio C., Maiolino R., Piconcelli E., Menci N., Aussel H., Lamastra A., Fiore F., 2010, A&A, 518, L155
- Gebhardt K., et al., 2000, ApJL, 539, L13
- Gibbon T. B., et al., 2015, Journal of Astronomical Telescopes, Instruments, and Systems, 1, 028001
- Golynkin A. A., Konovalenko A. A., 1991, Soviet Astronomy Letters, 17, 7
- Gültekin K., et al., 2009, ApJ, 698, 198
- Hardcastle M. J., Evans D. A., Croston J. H., 2006, MNRAS, 370, 1893
- Hardcastle M. J., Evans D. A., Croston J. H., 2007, MNRAS, 376, 1849
- Hardcastle M. J., et al., 2013, MNRAS, 429, 2407
- Hatch N. A., et al., 2011, MNRAS, 410, 1537
- Heiles C., Troland T. H., 2003, ApJS, 145, 329
- Hine R. G., Longair M. S., 1979, MNRAS, 188, 111
- Ho L. C., 2008, ARA&A, 46, 475
- Humphrey A., Villar-Martín M., Fosbury R., Vernet J., di Serego Alighieri S., 2006, MNRAS, 369, 1103
- Humphrey A., Villar-Martín M., Fosbury R., Binette L., Vernet J., De Breuck C., di Serego Alighieri S., 2007, MNRAS, 375, 705
- Inskip K. J., Best P. N., Longair M. S., Röttgering H. J. A., 2005, MNRAS, 359, 1393
- Inskip K. J., Villar-Martín M., Tadhunter C. N., Morganti R., Holt J., Dicken D., 2008, MNRAS, 386, 1797

- Intema H. T., 2014, preprint, ([arXiv:1402.4889](https://arxiv.org/abs/1402.4889))
- Intema H. T., van der Tol S., Cotton W. D., Cohen A. S., van Bemmel I. M., Röttgering H. J. A., 2009, *A&A*, 501, 1185
- Jackson N., Rawlings S., 1997, *MNRAS*, 286, 241
- Jansky K. G., 1933, *Popular Astronomy*, 41, 548
- Johnston S., et al., 2007, *PASA*, 24, 174
- Kaiser C. R., Best P. N., 2007, *MNRAS*, 381, 1548
- Kantharia N. G., Anantharamaiah K. R., 2001, *Journal of Astrophysics and Astronomy*, 22, 51
- Kazemi S., Yatawatta S., Zaroubi S., Lampropoulos P., de Bruyn A. G., Koopmans L. V. E., Noordam J., 2011, *MNRAS*, 414, 1656
- Kellermann K. I., Pauliny-Toth I. I. K., Williams P. J. S., 1969, *ApJ*, 157, 1
- Klamer I. J., Ekers R. D., Bryant J. J., Hunstead R. W., Sadler E. M., De Breuck C., 2006, *MNRAS*, 371, 852
- Kochanek C. S., et al., 2012, *ApJS*, 200, 8
- Konvalenko A. A., Sodin L. G., 1981, *Nature*, 294, 135
- Kormendy J., Richstone D., 1995, *ARA&A*, 33, 581
- Larson R. B., 2010, *Nature Physics*, 6, 96
- Magorrian J., et al., 1998, *AJ*, 115, 2285
- Marconi A., Hunt L. K., 2003, *ApJL*, 589, L21
- McCarthy P. J., van Breugel W., Spinrad H., Djorgovski S., 1987, *ApJL*, 321, L29
- Miley G., De Breuck C., 2008, *A&ARv*, 15, 67
- Moldón J., et al., 2015, *A&A*, 574, A73
- Motohara K., et al., 2000, *PASJ*, 52, 33
- Narayan R., Yi I., 1994, *ApJL*, 428, L13
- Ogle P., Whysong D., Antonucci R., 2006, *ApJ*, 647, 161
- Oonk J. B. R., et al., 2014, *MNRAS*, 437, 3506
- Payne H. E., Anantharamaiah K. R., Erickson W. C., 1989, *ApJ*, 341, 890
- Payne H. E., Anantharamaiah K. R., Erickson W. C., 1994, *ApJ*, 430, 690
- Pearson T. J., Readhead A. C. S., 1984, *ARA&A*, 22, 97
- Pentericci L., Röttgering H. J. A., Miley G. K., Spinrad H., McCarthy P. J., van Breugel W. J. M., Macchetto F., 1998, *ApJ*, 504, 139
- Pentericci L., Röttgering H. J. A., Miley G. K., McCarthy P., Spinrad H., van Breugel W. J. M., Macchetto F., 1999, *A&A*, 341, 329
- Pentericci L., et al., 2000, *A&A*, 361, L25
- Perley R. A., Napier P. J., Butler B. J., 2004, in Oschmann Jr. J. M., ed., SPIE Vol. 5489, *Ground-based Telescopes*. pp 784–795, doi:10.1117/12.551557

- Pilkington J. D. H., Scott J. F., 1965, *Memoirs of the RAS*, 69, 183
- Ponomarev V. O., Sorochenko R. L., 1992, *Soviet Astronomy Letters*, 18, 215
- Quataert E., 2001, in Peterson B. M., Pogge R. W., Polidan R. S., eds, *Astronomical Society of the Pacific Conference Series* Vol. 224, *Probing the Physics of Active Galactic Nuclei*. p. 71
- Reber G., 1949, *S&T*, 8
- Rodriguez-Rico C. A., Viallefond F., Zhao J.-H., Goss W. M., Anantharamaiah K. R., 2004, *ApJ*, 616, 783
- Roger R. S., Costain C. H., Stewart D. I., 1986, *AAPS*, 65, 485
- Röttgering H. J. A., Lacy M., Miley G. K., Chambers K. C., Saunders R., 1994, *AAPS*, 108
- Roy A. L., Goss W. M., Anantharamaiah K. R., 2008, *A&A*, 483, 79
- Ryle M., 1962, *Nature*, 194, 517
- Ryle M., Vonberg D. D., 1946, *Nature*, 158, 339
- Salem M., Brocklehurst M., 1979, *ApJS*, 39, 633
- Salgado et al. 2016a, *ApJ*, submitted
- Salgado et al. 2016b, *ApJ*, accepted
- Salvini S., Wijnholds S. J., 2014, *A&A*, 571, A97
- Sandage A., 1965, *ApJ*, 141, 1560
- Schilizzi R. T., 2005, in Gurvits L. I., Frey S., Rawlings S., eds, *EAS Publications Series* Vol. 15, *EAS Publications Series*. pp 445–463, doi:10.1051/eas:2005170
- Seaton M. J., 1964, *MNRAS*, 127, 177
- Shaver P. A., 1975a, *Pramana*, 5, 1
- Shaver P. A., 1975b, *A&A*, 43, 465
- Shaver P. A., 1978, *A&A*, 68, 97
- Shaver P. A., Churchwell E., Rots A. H., 1977, *A&A*, 55, 435
- Silk J., Nusser A., 2010, *ApJ*, 725, 556
- Smirnov O. M., Tasse C., 2015, *MNRAS*, 449, 2668
- Smith H. E., Spinrad H., 1980, *PASP*, 92, 553
- Storey P. J., Hummer D. G., 1991, *Computer Physics Communications*, 66, 129
- Tadhunter C., Morganti R., Rose M., Oonk J. B. R., Oosterloo T., 2014, *Nature*, 511, 440
- Taylor G. B., 2007, *Highlights of Astronomy*, 14, 388
- Tielens A. G. G. M., Miley G. K., Willis A. G., 1979, *AAPS*, 35, 153
- Tingay S. J., et al., 2013, *PASA*, 30, e007
- Urry C. M., Padovani P., 1995, *PASP*, 107, 803
- Varenius E., et al., 2015, *A&A*, 574, A114

- Varenius et al. 2016, A&A, submitted
- Villar-Martín M., Binette L., Fosbury R. A. E., 1999, A&A, 346, 7
- Villar-Martín M., Vernet J., di Serego Alighieri S., Fosbury R., Humphrey A., Pentericci L., 2003, MNRAS, 346, 273
- Viner M. R., Erickson W. C., 1975, AJ, 80, 931
- Walmsley C. M., Watson W. D., 1982, ApJ, 260, 317
- Werner N., et al., 2014, MNRAS, 439, 2291
- Whysong D., Antonucci R., 2004, ApJ, 602, 116
- Williams W. L., et al., 2016, preprint, (arXiv:1605.01531)
- Yatawatta S., et al., 2013, A&A, 550, A136
- Yun M. S., Ho P. T. P., Lo K. Y., 1993, ApJL, 411, L17
- van Haarlem M. P., et al., 2013, A&A, 556, A2
- van Weeren R. J., et al., 2016, ApJS, 223, 2